

Article

Methane and Ethane Steam Reforming over MgAl₂O₄-Supported Rh and Ir Catalysts: Catalytic Implications for Natural Gas Reforming Application

Johnny Saavedra Lopez , Vanessa Lebarbier Dagle, Chinmay A. Deshmane, Libor Kovarik, Robert S. Wegeng and Robert A. Dagle *

Institute for Integrated Catalysis, Pacific Northwest National Laboratory, 902 Battelle Blvd, Richland, WA 99352, USA

* Correspondence: Robert.Dagle@pnnl.gov

Received: 13 August 2019; Accepted: 19 September 2019; Published: 25 September 2019

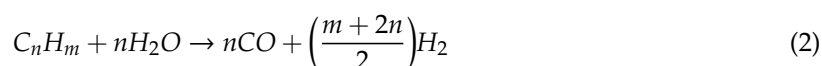


Abstract: Solar concentrators employed in conjunction with highly efficient micro- and meso-channel reactors offer the potential for cost-effective upgrading of the energy content of natural gas, providing a near-term path towards a future solar-fuel economy with reduced carbon dioxide emissions. To fully exploit the heat and mass transfer advantages offered by micro- and meso-channel reactors, highly active and stable natural gas steam reforming catalysts are required. In this paper, we report the catalytic performance of MgAl₂O₄-supported Rh (5 wt.%), Ir (5 wt.%), and Ni (15 wt.%) catalysts used for steam reforming of natural gas. Both Rh- and Ir-based catalysts are known to be more active and durable than conventional Ni-based formulations, and recently Ir has been reported to be more active than Rh for methane steam reforming on a turnover basis. Thus, the effectiveness of all three metals to perform natural gas steam reforming was evaluated in this study. Here, the Rh- and Ir-supported catalysts both exhibited higher activity than Ni for steam methane reforming. However, using simulated natural gas feedstock (94.5% methane, 4.0% ethane, 1.0% propane, and 0.5% butane), the Ir catalyst was the least active (on a turnover basis) for steam reforming of higher hydrocarbons (C₂₊) contained in the feedstock when operated at <750 °C. To further investigate the role of higher hydrocarbons, we used an ethane feed and found that hydrogenolysis precedes the steam reforming reaction and that C–C bond scission over Ir is kinetically slow compared to Rh. Catalyst durability studies revealed the Rh catalyst to be stable under steam methane reforming conditions, as evidenced by two 100-hour duration experiments performed at 850 and 900 °C (steam to carbon [S/C] molar feed ratio = 2.0 mol). However, with the natural gas simulant feed, the Rh catalyst exhibited catalyst deactivation, which we attribute to coking deposits derived from higher hydrocarbons contained in the feedstock. Increasing the S/C molar feed ratio from 1.5 to 2.0 reduced the deactivation rate and stable catalytic performance was demonstrated for 120 h when operated at 850 °C. However, catalytic deactivation was observed when operating at 900 °C. While improvements in steam reforming performance can be achieved through choice of catalyst composition, this study also highlights the importance of considering the effect of higher hydrocarbons contained in natural gas, operating conditions (e.g., temperature, S/C feed ratio), and their effect on catalyst stability. The results of this study conclude that a Rh-supported catalyst was developed that enables very high activities and excellent catalytic stability for both the steam reforming of methane and other higher hydrocarbons contained in natural gas, and under conditions of operation that are amendable to solar thermochemical operations.

Keywords: heterogeneous catalysis; syngas production; solar thermochemical; iridium catalyst; rhodium catalyst

1. Introduction

Approximately 95% of industrial hydrogen in the United States is currently produced through natural gas reforming [1,2]. The product of natural gas reforming is a mixture of H₂, CO, and CO₂, (referred to as syngas), which is a versatile and useful feedstock for producing a number of industrially relevant chemical commodities such as methanol, dimethyl ether [3], and Fischer-Tropsch products [4,5]. Natural gas reforming involves a series of reactions:



Reaction 1 is the steam methane reforming (SMR) reaction, which is endothermic and therefore requires high temperatures (e.g., 600–850 °C) for operation. Reaction 2 is the reaction for steam reforming of higher hydrocarbons (C₂₊). Both the SMR (Reaction 1) and water-gas-shift (Reaction 3) reactions are subject to thermodynamic equilibrium. Supported metal catalysts (e.g., Rh, Ru, and Ni metals supported on alumina or alumina spinel type formulations) are typically employed for steam reforming reactions [6,7].

Solar concentrators are a prospective method to provide the thermal requirements necessary to carry out the reforming process, with the added advantage of reduced carbon dioxide emissions since fossil fuel is not used to generate process heat [8–10]. Pacific Northwest National Laboratory has demonstrated an integrated solar thermochemical reaction system that combines solar concentrators with micro- and meso-channel reactors and heat exchangers that accomplish more than 20% solar augment of methane higher heating value. Further, a solar-to-chemical energy conversion efficiency slightly over 70% has been achieved [8]. At PNNL, the solar concentrators being utilized include those that provide concentration ratios high enough to achieve the temperatures required for methane steam reforming. These include parabolic dish concentrators and central receivers [8]. PNNL solar reformers typically operate in the 700–800 °C temperature range—with some portions of the reactor falling to less than 700 °C near the entry point to the reaction channel. PNNL solar reformers start reacting at modestly high temperatures (>600 °C) and exit the catalyst zone at substantiality at higher temperatures [8]. Typical steam/carbon (S/C) molar feed ratios utilized are in the 2.5–3.0 range. We routinely achieve 90% or greater conversion in on-sun testing under these conditions [8]. Catalysts used in these highly efficient compact reactors must meet the following requirements:

- They must be active over a wide range of operating temperatures, which are largely dictated by efficiency of the solar collector and local solar irradiance.
- To facilitate small reactor footprints, they must operate at high throughput rates.
- They must work under continuous shutdown cycles (i.e., sun/shade).
- To reduce energy requirements for steam vaporization, they must operate with reduced steam concentrations (e.g., low S/C molar ratios).
- They must tolerate temperature and gas composition changes caused by abrupt variations in local conditions.

Conventional Ni-based steam reforming catalysts have drawbacks pertaining to activity and durability that make them unsuitable for solar-driven applications. Noble metal-based catalysts, while generally more expensive than Ni-based catalysts, offer higher catalytic activities that enable faster throughput rates and smaller reactor hardware [11]. Furthermore, catalyst durability is improved, with reduced sintering and deactivation by coke when operating at the high temperatures required for typical operation [9]. Additionally, we note how, unlike with conventional fixed-bed reactor systems, with microreactors the use of more expensive precious metal catalysts may be made economical. Monolith-type substrates utilizing highly active catalysts are integrated in microreactors to minimize

heat- and mass-transfer resistances and maximize catalyst efficiency. The use of smaller, more efficient systems may compensate for the higher cost of the catalyst material [12].

SMR catalysts commonly employ Ni or Rh metals and use alumina or alumina spinel (e.g., MgAl_2O_4) type supports [13–15]. SMR is a structure-sensitive reaction in which turnover rates increase with decreasing metal particle size [16,17]. The support choice influences both the resulting metal particle size and catalyst stability [17,18]. Facilitating increased metal dispersion and enabling improved stability are among the reasons for using MgAl_2O_4 over other common supports (e.g., Al_2O_3 , SiO_2 , and ZrO_2). Noble metal based catalysts are known to be more resistant to carbon fouling and metal sintering compared to Ni [19–21]. We have previously reported MgAl_2O_4 -supported Rh and Ir catalysts to have improved activity and stability compared to Ni and other metals (e.g., Pd, Pt) [20]. Catalysts with very well dispersed Rh (2 nm) and Ir (1 nm) metal clusters were obtained with the use of a MgAl_2O_4 support. High dispersion was maintained even after high temperature operation (e.g., 850 °C) and with the use of high metal loadings (e.g., 5–10 wt.%). Taken together, well dispersed Rh and Ir catalysts with high metal loadings were previously reported by our group to be highly active and stable for the SMR reaction.

While methane is the predominant compound in natural gas, natural gas also contains up to 20 vol.% higher C_{2+} constituents, with the exact composition depending on the source [22,23]. The activation of methane requires a higher temperature than required for activation of C_{2+} natural gas components [24]. Thus, C_{2+} hydrocarbons are typically converted more readily when compared to methane. However, C_{2+} hydrocarbons facilitate coke formation [25,26]. Regardless of the hydrocarbon used, upon reaction the metal and metal oxide support surfaces are populated by a variety of reactive species (e.g., C^* , H^* , CH_x^* , CO^* , O^* , OH^*) [8,27–33]. While SMR has been studied extensively, relatively few studies have been dedicated to studying its reaction mechanism when higher hydrocarbons are present in the feed, which would be more representative of real feed mixtures [19,21,31,34,35]. The presence of higher hydrocarbons facilitate catalyst deactivation [25,26]. Previously, we investigated steam reforming of biomass gasifier-derived hydrocarbons, which includes tar (polyaromatic hydrocarbons) species. We evaluated steam reforming of benzene, as a model tar species, over MgAl_2O_4 -supported Rh and Ir catalysts. The Rh catalyst was more active than Ir on a turnover basis due to differences in the C–C bond breaking step (which was found to be rate limiting) [19].

The objective of this study is to assess the catalytic performance of Rh-, Ir-, and Ni-supported catalysts for steam reforming of natural gas. Both Rh- and Ir-based catalysts are known to be more active and durable than conventional Ni-based formulations, and recently Ir has been reported to be more active than Rh for methane steam reforming on a turnover basis [20,36]. Thus, the effectiveness of all three metals to perform natural gas steam reforming was evaluated in this study. Steam reforming kinetic and mechanistic comparisons were elucidated using both discrete methane and ethane feeds. While the catalytic performance of various precious metal based catalysts (i.e., Rh, Ir, and Ni) have been widely studied for the methane steam reforming reaction, we are not aware of any studies focused on their comparison when under ethane steam reforming conditions. Finally, we comparatively assess both activity and stability when using a simulant natural gas feedstock that was a mixture of methane and C_{2+} hydrocarbons. We note that in order to investigate the kinetics of the catalysts we are operating at higher throughputs and lower conversions than what are typically utilized in solar thermochemical application.

2. Results and Discussion

The performance of MgAl_2O_4 -supported Rh, Ir, and Ni catalysts was investigated for steam reforming of natural gas under industrially relevant conditions. The methods explored included the use of (1) simulated natural gas feedstock, (2) separate methane and ethane model feeds to elucidate contributions from each, (3) catalyst durability tests, and (4) evaluation over a wide temperature range. These conditions are all of particular interest for solar thermochemical applications where highly active and durable catalysts are required for a range of conditions.

2.1. Catalyst Characterization

Catalyst physical characterization details are presented in Table 1. These MgAl₂O₄-supported metal catalysts have been characterized in our previous publications, and used as catalysts for steam reforming of methane [20], gasifier-derived hydrocarbons including benzene [19] and complex mixtures including tar [21], and biomass-derived ethylene glycol [37] and aqueous products produced via fast pyrolysis [38]. It was reported that the metals form small and stable clusters when supported on MgAl₂O₄ (approximately 1, 2, and 7 nm Ir, Rh, and Ni median cluster sizes, respectively) even under steam reforming conditions at 850 °C [20,21]. In this study, we report additional catalyst characterization include TPR as well as the hydrogen adsorption over the temperature range of interest for natural gas steam reforming (i.e., 600–850 °C).

Table 1. Catalyst physiochemical characterization. Scanning transmission electron microscopy (STEM) images for the Ir and Rh catalysts are included in the supplementary information (Figure S1).

| Catalyst | Metal Loading (wt.%) | Metal Particle Size TEM (nm) | Catalyst Surface Area BET ^a (m ² /g) |
|--------------------------------------------|----------------------|------------------------------|------------------------------------------------------------|
| 5Ir/MgAl ₂ O ₄ [20] | 5.0 | 1.0 | 133 |
| 5Rh/MgAl ₂ O ₄ [20] | 5.0 | 2.0 | 117 |
| 15Ni/MgAl ₂ O ₄ [21] | 15.0 | 6.6 | 86 |

^a Brunauer–Emmett–Teller method.

Figure 1 shows TPR profiles for the Rh-, Ir-, and Ni-supported catalysts used in this study. Results indicate an easier reduction for Rh with a single reduction peak at 112 °C. Ni requires the highest temperature to reach a similar reduction level (peak centered at 725 °C) and shows evidence of at least two reduction stages (shown by overlapping peaks). The Ir catalyst shows several reduction stages at 168, 220, 253, and 613 °C. For all the three catalysts (Rh, Ir, and Ni) after 800 °C was reached, no further hydrogen was chemisorbed, indicating a total (or near total) reduction of the metal clusters. However, the temperature needed to produce reduced metal clusters (measured by hydrogen consumption) varied significantly. Results in the literature suggest Rh disperses very well on a wide variety of supports, with low temperature single peaks being characteristic for Rh [39,40], thus corroborating our results. The several reduction stages required for Ir can be ascribed to a broader particle size distribution or a broad distribution of oxidation states. Reports in the literature indicate that smaller Ir particles require a higher reduction temperature compared to those for larger particles [41,42]. Nevertheless, the reduction of Ir-based catalysts is a relatively complex phenomenon that largely depends on the processing conditions and thermal history of each sample (Ir reduction is an autocatalytic process and IrO_x are volatile species detrimental to metal dispersion) [43]. The Ni catalyst TPR profile also is consistent with literature results for catalysts with a similar particle size (6 nm) [44,45]. Before reaction catalysts are reduced at 850 °C for 16 h in order to ensure a degree of reduction for the metal clusters. We note that in our prior reports we have shown how the MgAl₂O₄-supported Ir, Rh, and Ni clusters are fully reduced when the catalyst was reduced under hydrogen at 850 °C. However, we note that the total reduction cannot be determined, especially for Ni (because of its lower dispersion), when under operando conditions.

H₂ activation, adsorption strength relative to carbon, and coverage on metal surfaces are important metrics for steam reforming relevant reactions [33,41,46]. However, obtaining accurate characterization under operando conditions presents technical and experimental challenges. In an attempt to study H₂ adsorption capacity relative to metal active area, we combined volumetric H₂ adsorption at 600 °C (as representative of reforming conditions) with metal dispersion, as determined from metal particle sizes revealed by the STEM imaging (2 nm, 1 nm, and 7 nm for the Rh, Ir, and Ni, respectively) [20,21]. The H₂ adsorption data presented in Figure 2 was calculated as H-coverage evolution (mol_H/mol_{Msurf}, M= Rh, Ir, Ni) for accumulated H₂ added (by pulses) into the adsorption cell (μmol). These adsorption results indicate that bare Rh and Ir surfaces adsorb H₂ completely until saturation, which is indicated

by the inflexion point and the asymptotical part of the plots (after adding ~40 and ~20 mmol of H₂, respectively). Saturation is reached at coverages of H-M_{surf} of 1 and 0.7 for Rh, and Ir, respectively, which indicates a surface stoichiometry of 1:1 (H:Rh_{surf}) and 0.7:1 (H:Ir_{surf}). In the case of Ni, the adsorption pattern is dissimilar in three main aspects: (1) H-uptake is low (0.2 mol_H/mol_{Ni_{surf}}) compared to Rh or Ir, (2) there is no clear inflexion point for the adsorption curve, and (3) the calculated stoichiometry H-Ni_{surf} is low (only 20% of surface nickel atoms adsorb hydrogen). H₂-uptake at 800 °C is lower compared to the uptake at 600 °C (data shown Figure S2). At 800 °C, hydrogen saturates the metal surfaces at 1:1 (Rh), 0.5:1 (Ir), and 0.08:1 (Ni).

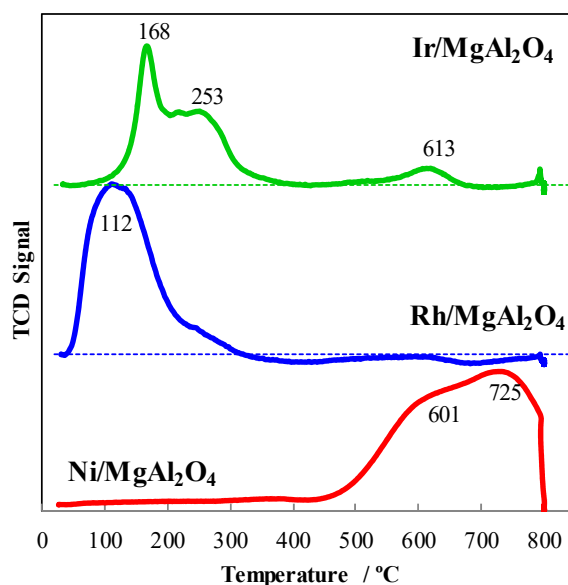


Figure 1. Temperature programmed reduction (TPR) profiles for MgAl₂O₄-supported Ir, Rh, and Ni catalysts. Prior to TPR the catalysts were calcined at 500 °C for 4 h. TPR conditions were 50 mg of catalyst, temperature ramping rate 5 °C/min, feed rate of 50 mL/min of 5% H₂/Ar gas.

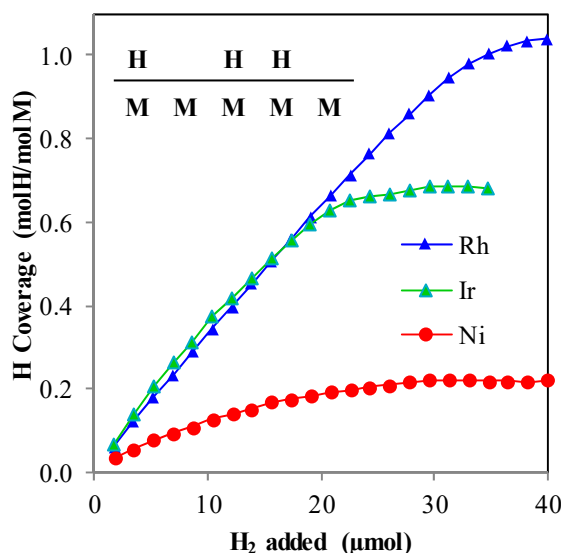


Figure 2. Hydrogen surface saturation curves over MgAl₂O₄-supported Rh (blue), Ir (green), and Ni (red) catalysts at 600 °C. Coverage was calculated using accumulated H₂-uptake and metal dispersion data obtained from STEM imaging (Table 1). 50 mg of catalyst was calcined before analysis and reduced at the conditions used in the catalytic experiments (16 h at 850 °C, 100 mL/min, 10% H₂ in N₂). H₂ was pulsed using a 100 μL gas loop.

The physicochemical characterizations of the catalysts shown in this section are significant for the following reasons:

- STEM characterization shows that high dispersion that can be achieved with Rh and Ir catalysts supported on MgAl_2O_4 compared to Ni.
- TPR characterization showed that, associated with a greater dispersion, reducibility is enhanced, particularly for Rh where TPR profiles indicate a narrower particle size distribution and full reduction at low temperatures (broad single peak centered at 112 °C).
- H_2 adsorption demonstrated that surface stoichiometry for H_2 on metal surfaces can vary greatly under reforming conditions.

We found that while full surface coverage with a stoichiometry 1:1 $\text{H-Rh}_{\text{surf}}$ can be achieved at reforming temperatures in the 600–800 °C range for the Rh catalyst, this coverage is significantly lower for Ir (0.7:1 $\text{H-Ir}_{\text{surf}}$) and even lower for Ni (0.2:1 $\text{H-Ni}_{\text{surf}}$).

2.2. Steam Reforming Activity Comparison Using Natural Gas Simulant

Steam reforming using a simulant gas mixture representative of natural gas (94.5% methane, 4% ethane, 1% propane, 0.5% butane) was performed over MgAl_2O_4 -supported 5% Ir and 5% Rh catalysts. Conversion of methane and ethane is plotted separately and shown in Figure 3 (propane conversion in Figure S3). Short contact times ($\tau = 4.5$ ms) favor low conversion levels. In the 600–875 °C temperature range, methane conversion follows a linear trend for both catalysts (Figure 3a). In spite of similar methane conversion, conversion of ethane (Figure 3b) and propane (Figure S3) is significantly lower for the Ir catalyst in the lower temperature range (<750 °C). These differences in activity are important for two main reasons: (1) gas feeds with higher concentration of C_{2+} hydrocarbons lower the overall performance of Ir-based catalysts (more hydrocarbons remain unreacted) and (2) hampered hydrocarbon hydrogenolysis/reforming activity is an indication that the underlying mechanism is different for Ir compared to Rh in spite of similar methane reforming activity. We note that the methane conversions presented in Figure 3a are below those of equilibrium (with the equilibrium conversions indicated with the dotted line). We also note that the equilibrium ethane conversion shown in Figure 3b is near completion for the entire range of conditions investigated.

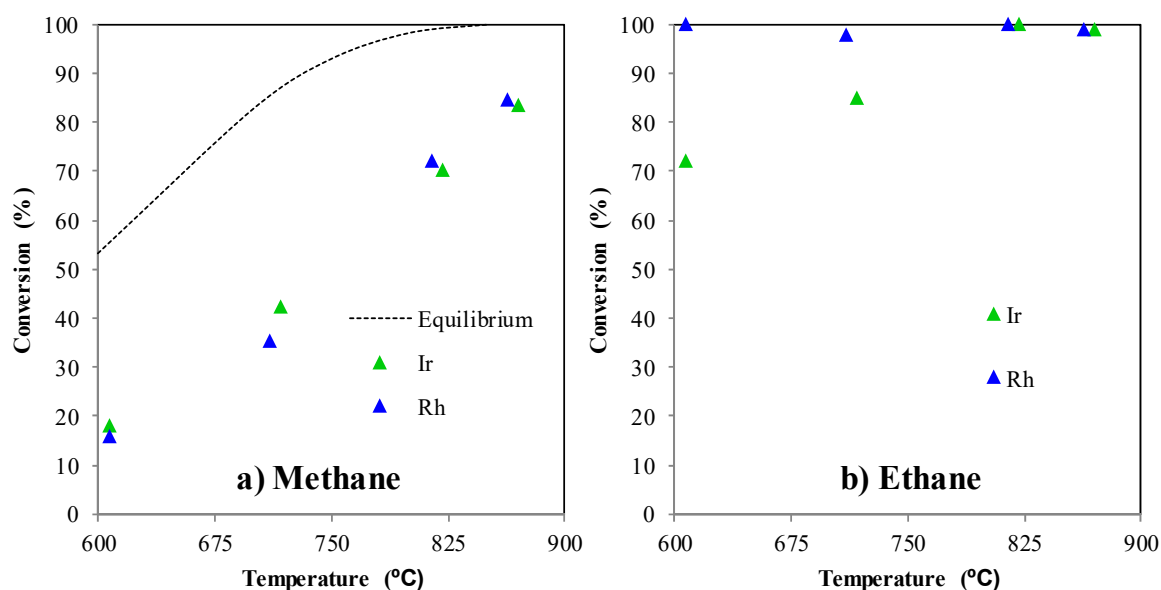


Figure 3. Comparison of (a) methane conversion and (b) ethane conversion for the Rh and Ir catalysts when steam reforming using natural gas simulant feedstock ($S/C = 1.5$ mol, $\tau = 4.5$ ms).

We note that H_2/CO ratio is an important metric for reforming catalysts when the steam reforming reaction is integrated to downstream processes. In practice, several strategies can be used to tune the H_2/CO ratio of the reforming product (e.g., decreased S/C ratio during SMR, CO_2 recirculation, incorporating an additional WGS step) towards reactions of interest (e.g., Fischer–Tropsch). The H_2/CO ratio for $RhMgAl_2O_4$ was evaluated over a wide range of conversions (20%–100%) at the range of operative temperatures of SMR in solar thermochemical applications (600–800 °C) by changing the contact time of the methane stream (for τ values from 1.2 to 10 ms) at a constant S/C ratio (S/C = 3). Results for conversion vs. temperature, and H_2/CO ratio vs. conversion are presented in the supplementary information as Figure S8. Interestingly, Figure S8 shows that independently on the temperature, H_2/CO ratio decreases exponentially with methane conversion reaching a minimal value of 5 at the highest conversion (ca. 100%). This will lead to the conclusion that WGS equilibrium determines the resulting H_2/CO ratio. As the H_2 partial pressure increases as an effect of higher reforming conversion, more CO is formed through the reverse water gas shift reaction (RWGS, $CO_2 + H_2 \rightarrow CO + H_2O$).

2.3. Methane and Ethane Steam Reforming Activity Comparison

Based on the results described above, the Ir catalyst shows lower activity than Rh towards the steam reforming of higher hydrocarbons. With the aim of gaining knowledge on fundamental differences between the different hydrocarbon constituents, we performed a set of separate experiments using either methane or ethane feed. Figure 4 shows the metal surface normalized catalytic rate ($\text{moles}_{CH_4}/\text{mol}_{\text{metal}} \cdot \text{s}$) for the steam reforming of methane and ethane for the Rh, Ir, and Ni supported catalysts as a function of temperature. These results show that for the Ir catalyst, the ethane steam reforming rates (Figure 4b) are significantly lower compared to methane steam reforming rates (Figure 4a). For the Rh and Ni catalysts, ethane conversion is more facile than methane conversion.

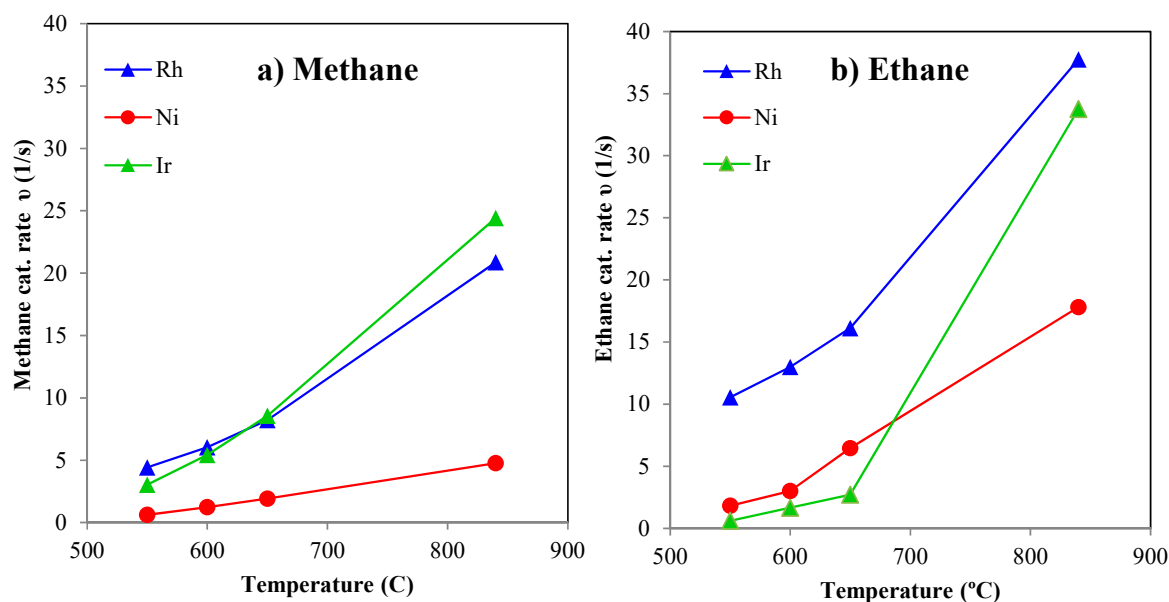


Figure 4. Comparison of turnover steam reforming rates for the Rh, Ir, and Ni catalysts using (a) methane, and (b) ethane feeds (S/C = 3, τ = 30 ms; methane feed = 15.9 vol%, ethane feed = 14.8 vol%).

Over typical metal supported catalysts activation of the initial C–H bond of methane is more difficult than for ethane [47]. Dehydrogenation of the initial C–H and the creation of C radical + H for ethane is slightly more favorable than for methane (C–H bond strength 101 vs. 105 kcal/mol, respectively). Further, the C–C bond of ethane is much weaker (90.1 kcal/mol) [48]. These differences between methane and ethane typically make ethane more reactive than methane. Few literature studies can be used to make a direct comparison or to determine trends with respect to reactivity of methane

vs. ethane reforming because most studies use methane as the only model reactant. Specific studies on ethane reforming have yielded contradictory results depending on the metal used as the catalyst. On one hand, Schädel et al. [35] showed that over Rh, ethane reacts faster than methane, which is consistent with our findings for Rh and Ni catalysts. On the other hand, Graf et al. [34] reported that over Pt, methane reforming occurs the fastest, which is similar to our findings for Ir. Similar trends, where ethane reactivity is higher compared to methane, have been found in other metal-catalyzed reactions such as ethane combustion [49] and ethane hydrogenolysis over Pt and Pd [50]. Interestingly, Figure 3b also shows that the Ir catalyst is relatively inactive at low temperatures but then the catalytic rates quickly accelerate at higher temperatures (>750 °C). This rapid transition from ‘inactive’ to ‘active’ prompted our study to pursue a more detailed understanding for ethane reactivity over Ir catalyst. The following section is dedicated to hypothesizing the possible reason(s) behind the low reactivity of ethane over Ir catalysts at temperatures lower than 750 °C.

2.4. Ethane Steam Reforming over Rh vs. Ir: Mechanistic Insights

Results shown in Figure 4 indicate that over Ir catalyst at 600 °C, surface normalized ethane reforming rates (0.6 s^{-1}) are much slower compared to methane reforming rates (3 s^{-1}). This difference in catalytic rate could be attributed to several factors: (1) potential formation of carbon deposits over Ir surface when ethane is fed, (2) decreased number of active sites due to competitive adsorption (e.g., ethyl, O, OH, H, C₁, and C₂ species), and the (3) chemical identity of the metal and its bonding characteristics. To compare hydrocarbon reactivity over metal surfaces, catalytic measurements should be performed under the same coverage [51]; however, this comparison is not always easy to achieve. As a simplified approach to compare ethane reforming activity over Ir vs. Rh, we performed catalytic measurements at 600 °C using the same concentration of ethane in the gas over similar amounts of metal exposed (Table 2). The average Rh cluster size (2 nm) was twice that of the Ir cluster (1 nm); however, the Ir molecular weight (192 g/mol) is twice that of Rh (103 g/mol). Thus, the amount of exposed metal is similar for both catalysts on a molar basis. With similar number of exposed metal sites, the observed product selectivity and associated reaction rates should be determined by the underlying chemical reaction mechanism.

Table 2. Catalytic results for ethane steam reforming over MgAl₂O₄-supported Rh and Ir catalysts at 600 °C (S/C = 2.75 mol, τ = 28.3 ms).

| Condition | 5%Rh/MgAl ₂ O ₄ | 5%Ir/MgAl ₂ O ₄ |
|------------------------------------------------------------|---------------------------------------|---------------------------------------|
| Metal on catalyst surface (μmol) ^a | 23.5 | 25.2 |
| Conversion after 1 h | 60.0 | 8.3 |
| Conversion after 2 h | 58.9 | 8.1 |
| Deactivation rate (%) | 1.8 | 2.4 |
| ppm ethylene formed | 50 | 2000 |
| Selectivity towards methane (mol C %) | 32 | 9.6 |
| Carbon on spent catalyst (wt.%) | bdl ^b | 2.8 ^c |

^a Based on TEM particle size measurements. ^b Below limit of detection of CNHS elemental analysis instrument (0.3%). ^c 0.28% measured for the dilution of 1:10 catalyst:Al₂O₃.

Shown in Table 2 are ethane steam reforming results using the Rh- and Ir-supported catalysts. For both catalysts steady state is reached after 15 min, and catalytic activity is reported after 1 h and 2 hours’ time-on-stream (see Figure S4). The main reaction products detected by gas chromatography analysis include H₂, CO₂, CO, methane, and ethylene. Reactivity of ethane over Rh is different than Ir in four main aspects: (1) conversion is significantly higher (60% vs. 8%), over a similar exposed metal surface area, (2) ethylene formation is markedly lower (50 ppm vs. 2000 ppm), (3) post mortem analysis showed significant less accumulated carbon, and (4) methane is the main reaction product (methane selectivity of 32% vs. 9.6%).

Methane is the primary hydrocarbon product over Rh when under ethane steam reforming conditions. Methane can be formed as a hydrogenation product of CO or CO₂ [33] or as a product of ethane hydrogenolysis (according to the Sinfelt–Taylor mechanism) [52,53]. These two reactions are related and depend on the metal's carbon/hydrogen adsorption characteristics and its ability to breakdown adsorbed C₂ radicals [54]. In Section 3.1 we reported marked differences in H₂ adsorption and coverage for the Rh catalyst vs. Ir or Ni. Although the H₂ adsorption experiment does not allow comparison for H/C adsorption, they demonstrate improved H retention for the Rh catalyst. This is a particularly useful property that favors the aforementioned methane formation mechanisms (hydrogenation of CO/CO₂ species and hydrogenolysis of ethane) under reforming conditions. Parallel to methane formation, the presence of ethylene product is an indicator of formation (and slow decomposition) of ethyl radicals on the catalyst surface. Higher formation of ethylene over the Ir catalyst is a strong indicator that the overall catalytic ethane reforming rate is hampered by a slow C–C bond scission capacity compared to Rh.

The marked difference in conversion for the Ir and Rh catalysts shown in Table 2 makes it difficult to fairly compare product selectivity. Conversion for the Ir catalyst was increased, by increasing the contact time (from 28 to 166 ms), to compare product selectivity at similar conversion levels. As shown in Figure 5, under these conditions methane is the main reaction product for both catalysts (60% vs. 30% methane selectivity for Ir and Rh, respectively), with CO and CO₂ also being produced as main products, and ethylene being produced via incomplete decomposition of ethane. Figure 5c shows changes in selectivity as a function of change in contact time over the Ir catalyst. Methane selectivity increases as ethane conversion increases (selectivity towards methane increases from 8 to 31% for ethane conversion increasing from 8 to 50%). Interestingly, selectivity towards ethylene formation decreases as the conversion increases (2 to 0.6%), which is significantly higher than selectivity towards ethylene over the Rh catalyst at a similar conversion (0.02%, Insert in Figure 5c). These changes in product selectivity—increased methane and decreased ethylene—at higher ethane conversion levels can be explained in a scenario where C–C bond scission forming methane is the main and primary route for ethane decomposition before reforming reactions (CO and CO₂ formation) take place, and is similar for both metals (Figure S5).

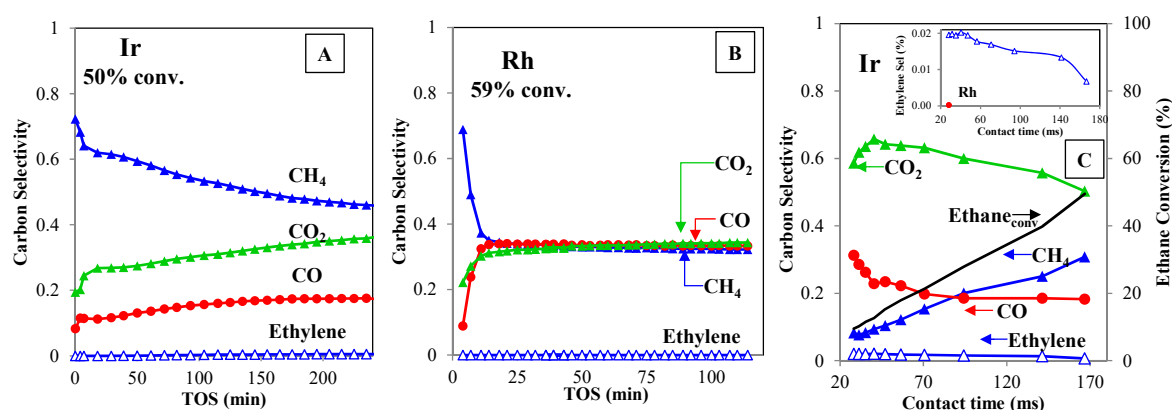


Figure 5. Product selectivity for ethane steam reforming at 600 °C (S/C = 2.75 mol, τ = 28 ms [Rh]; τ = 167 ms [Ir]; ethane feed = 16 vol %) over Ir/MgAl₂O₄ catalyst at 50% ethane conversion (A), over Rh/MgAl₂O₄ catalyst at 59% ethane conversion (B). Variation of carbon selectivity with ethane contact time over Ir/MgAl₂O₄ catalyst (C).

These observations for ethane reforming over Ir compared to Rh (higher ethylene formation, lower selectivity towards methane) can be combined to suggest that hydrogenolysis of ethane is relatively slow over Ir and facile over Rh. This hypothesis is additionally supported with several control experiments performed over Ir catalyst and summarized into the following four main points:

- (1) Ethane steam reforming rate does not increase with higher S/C ratios. A wide range of S/C ratios were used to eliminate oxidation (reforming steps) as being responsible for the lower reaction rate on Ir (S/C up to 10). This is illustrated in Figure 6. This result is consistent with kinetic literature studies reporting that the reforming reaction is independent of the partial water pressure (zero order with respect to water) [36].
- (2) Low activity over Ir catalyst is not caused by coke formation. In spite of higher carbon content on Ir spent catalyst (Table 2), coke (or at least hard coke) is not formed. A series of control experiments showed that high activity is consistently low for ethane reforming after repeated methane/ethane cycles (see Table S1).
- (3) Lower ethane partial pressure increases catalytic conversion. This is consistent with hydrocarbon hydrogenolysis literature reporting that hydrocarbons equilibrate with metal surfaces by sequential dehydrogenation steps. As a consequence, a lower ethane partial pressure (from 14 to 8 mol %) causes a lower coverage that increases the number of active sites (ethane conversion increases from 10 to 47%).
- (4) Ethane reforming over Ir supported on Al_2O_3 shows similar trends. Ir supported by Al_2O_3 is active for methane reforming; however, ethane steam reforming is severely hampered. Ir supported on alumina has a bigger particle size (4 nm) [20].

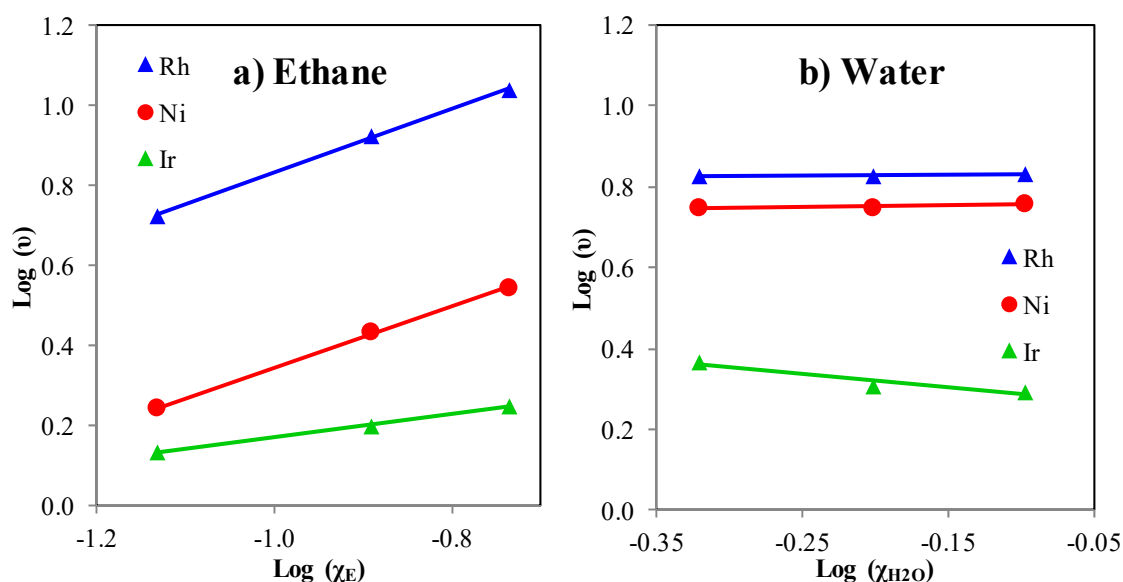


Figure 6. Logarithmic plot for catalytic rate vs. partial pressure of (a) ethane and (b) water.

2.5. Ethane Reforming Kinetic Measurements

Methane reforming kinetics have been extensively reported in the literature. Results indicate that methane decomposition and reforming rates are first order in methane; C–H activation is the rate limiting step and occurs on metal surfaces similar to conventional hydrocarbon chain reaction mechanism [32,55]. Ethane activation over metal surfaces is more complex, involving a series of partially dehydrogenated intermediates that lead to C–C bond breaking [41,56]. Strongly adsorbed H is considered to be competitive with hydrocarbon adsorption and limits its reactivity (in general, and over metal surfaces, the ethane hydrogenolysis rate is inhibited by excess H_2) [50,57,58]. One might think that interaction of highly dehydrogenated species in the absence of active hydrogen could lead to a higher coke formation; however, there is limited experimental evidence that shows that co-feeding hydrogen prevents coke formation better than water does [59]. Regarding the activation of the oxidant (e.g., steam), it is been largely reported that methane has zero order dependence on water (or CO_2). This indicates that after C–H activation, all the catalytic steps, including dehydrogenation of CH_x species, CO/CO_2 formation, and WGS reaction, should have no kinetic relevance.

To study the influence that the concentrations of reactants have in catalytic rate, we varied ethane and water concentrations in the gas feed at 600 °C. Kinetic results for catalytic rate vs. partial pressure are shown in Figure 6. Calculated reaction orders for both ethane and water and activation energies are shown in Table 3. The reaction order to ethane is less than one and zero or near zero to water. For methane steam reforming, the reaction is first order to methane, and the rate limiting steps have been found to be adsorption and activation of the C–H bond [36]. Thus, there is less dependence of hydrocarbon partial pressure on reaction rate for ethane steam reforming than for methane steam reforming.

Table 3. Kinetic parameters calculated for ethane steam reforming reaction at 600 °C.

| Catalyst | n_{Ethane} | n_{water} | E_a (kJ/mol) ^a |
|-------------------------------------|---------------------|--------------------|-----------------------------|
| Rh/MgAl ₂ O ₄ | 0.79 | 0 | 26.8 |
| Ni/MgAl ₂ O ₄ | 0.76 | 0 | 79.1 |
| Ir/MgAl ₂ O ₄ | 0.29 | −0.3 | 95.7 |

^a Measured at 550, 600, and 650 °C.

The results presented in Table 2 indicate that the Ir catalyst accumulated more carbon on the surface than Rh after the ethane reforming reaction at 600 °C; this presumably is due to a slower C–C scission rate. Analysis of the hydrogenolysis mechanism suggests that if a surface step is hampering the catalytic cycle, the initiation step (adsorption/activation of C–H bond) loses kinetic importance (resulting in a lower reaction order). Our low reaction orders for the Ir catalyst ($n_{\text{ethane}} = 0.29$ and $n_{\text{water}} = -0.3$) are consistent with high carbon coverage of the catalyst surface; in this catalyst, the reaction of adsorbed H with C₂ species occur before the C–C bond breaking step, causing formation of ethylene gas. In the ethane hydrogenolysis reaction, the hydrogen adsorption capacity of the metal (M–H coordination), its adsorption strength, and the coverage relative to other species (C₂, C₁) are important factors in overall catalytic rate and coke formation. The initiation and termination reactions in hydrocarbon chain mechanisms on metals require a high affinity of the metals for H. Our previous analysis in this section indicate that the slowest step is related to the creation (and accumulation) of adsorbed carbon species (C₁ and C₂); these results might be related to a poor capacity to activate and retain H. The low reaction order found for ethane reforming (0.29), a higher ethylene formation level, and higher carbon accumulation (Table 2) support the conclusion that surface ethyl decomposition (part of ethane hydrogenolysis reaction) is superseding the global reaction order.

Ethane steam reforming studies at 600 °C on Rh performed by Graf et al [59] indicated that in the presence of H₂, ethane reacts to form methane at a much higher rate than towards the formation of reforming products; additionally, their analysis of reaction products suggests that ethane reforming and hydrogenolysis proceed in a parallel fashion. Our analysis of reforming products differs in two important key aspects from the conclusions by Graf et al. First, by changing the contact time, we found that a higher ethane conversion is accompanied by a higher selectivity towards methane and a lower formation of ethylene (Figure 5c, Figure S5). This indicates that hydrogenolysis reaction proceeds reforming reactions; in other words, reforming steps are sequential to ethane hydrogenolysis. Second, the amount of H available and its adsorption strength to hydrogenolysis reaction becomes critical, more than what it is the presence of oxidant species [41,58]. In this scenario, surface active hydrogen is necessary to hydrogenate C₁ species on catalyst surface that will cause excessive carbon buildup if they don't undergo reforming reactions. Several key factors for improved catalysis are (1) an optimal amount of steam, (2) a fast C–C bond scission rate, and (3) a high H retention capacity by the catalyst. These key factors will avoid the accumulation of highly dehydrogenated carbon species (especially C and CH [80 kcal/mol]) that promote coke formation.

2.6. Catalyst Stability

Catalyst longevity is one of the cornerstones in the study of reforming catalysts. Sintering of metal particles, loss of support surface area, and extensive coke formation can cause catalyst fouling at the harsh conditions necessary to perform reforming reactions. Spinel supported metals (especially Ir and Rh) have been shown to maintain physical stability under these harsh reaction conditions with minimal coke formation [20,21]. In this section, we analyze the effect that the use of a simulant natural gas has in catalyst performance, focusing on longer term stability. In the prior sections we demonstrated that C_{2+} steam reforming activity is limited over Ir-based catalysts, presumably due to a reduced capacity of breaking ethane's C–C bond becoming rate limiting at low reaction temperatures. In the following section, we present results for the Rh catalyst (chosen as benchmark) and evaluate the influence that reaction conditions have on catalyst performance. The aim is to find reaction conditions that allow stable catalytic operation even with fast throughputs and relatively low S/C ratios.

For the reforming experiments shown in Figure 3, methane was fed at a rate of 5.3 mmol/min and the reaction was carried out on similar metal surfaces (23.5 and 25.2 μmol of Rh and Ir respectively). The catalytic rate was reported for each temperature after 1 h where steady state was reached. Using these reaction conditions, especially with short reaction times (1 h time on stream [TOS]), no deactivation was seen; however, if the reaction was allowed to proceed for longer times, deactivation was evident. The results shown in Figure S6 (for the reaction at 850 °C) show how conversion starts to decline slightly after 8 h of reaction. Under ethane reforming conditions, a more pronounced deactivation was found after a few hours on stream for the reaction at 600 °C (see Table 1). It is clearly evident that the presence of C_{2+} hydrocarbons, and especially at a high carbon throughput, has a negative effect on catalyst life, which largely depends on the reaction temperature and feed rate.

Catalyst durability experiments for methane steam reforming over the Rh catalyst are presented in Figure 7a. After over 100 h at both 850 and 900 °C ($\tau = 2.3$ ms, $S/C = 2$), no deactivation was observed. Figure 7b depicts results when using a simulated natural gas feed mixture containing methane, ethane, propane, and butane. For simplicity, only methane conversion results are shown in Figures 7b and 8. After 100 h, catalysts showed continued deactivation and retention of only part of the initial activity (91%, 78%, and 53% activity retained for the Ir, Rh, and Ni catalysts, respectively). These results illustrate how the presence of C_{2+} hydrocarbons are detrimental to catalyst durability. However, we note that these results were obtained at a very low molar S/C ratio of 1.5. We attribute catalyst deactivation to increased carbon fouling (coke buildup) of the higher hydrocarbons on the catalyst surface. As shown in Figure 7c when the molar S/C feed ratio was increased to 2.0 the catalyst was quite stable at 850 and even 900 °C for 120 h duration. Although we note that prolonged duration testing at 900 °C revealed some deactivation, at 850 °C the reaction was quite stable.

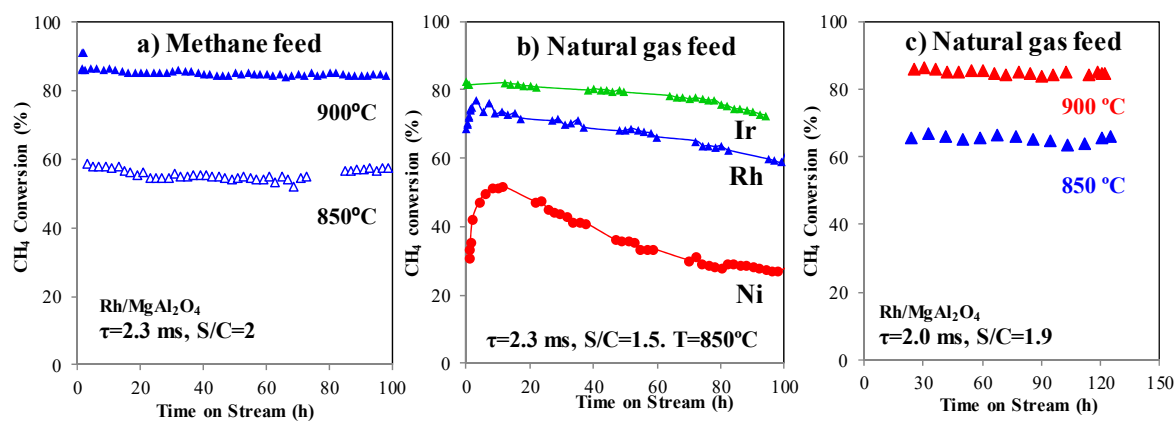


Figure 7. Methane conversion vs. time on stream (TOS) using (a) pure methane feed over Rh at 850 and 900 °C ($S/C = 2.3$ ms, $\tau = 2.3$ ms), and using natural gas simulant feed over (b) Rh, Ir, and Ni at 850 °C ($S/C = 1.5$ ms, $\tau = 2.3$ ms), and (c) Rh at 850 and 900 °C ($S/C = 1.9$ ms, $\tau = 2.0$ ms).

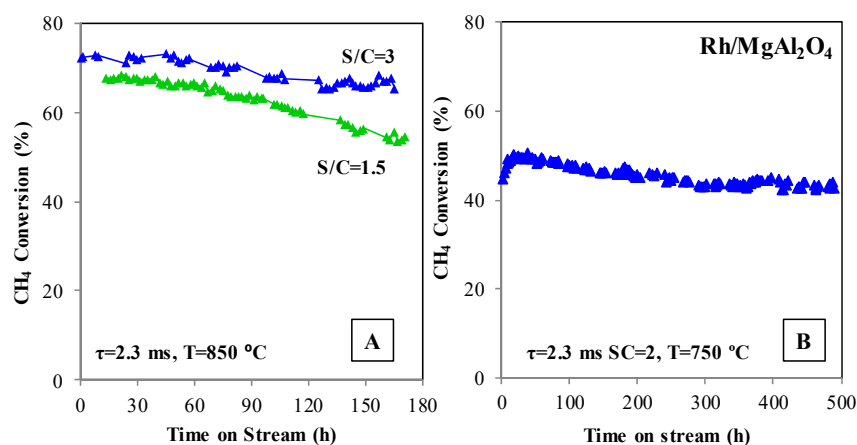


Figure 8. Methane conversion vs. TOS over Rh/MgAl₂O₄ catalyst as a function of steam/carbon molar feed ratio at 850 °C (A), and at 750 °C for 500 h TOS (B).

There are two common strategies for avoiding/suppressing coking on reforming catalysts: (1) increase the amount of steam fed and (2) conduct the reaction at lower temperatures. On one hand, increasing the amount of steam increases the formation of oxidation products (CO, and CO₂), while hydrocarbon adsorption/activation rates remain unaffected. On the other hand, the main effect of a lower reaction temperature is a decrease in the rates of hydrocarbon activation; as a result, reforming reaction rates supersede the coke rate formation, finally leading to a more stable long-term operation. Results for these two situations are presented in Figure 8 for the Rh catalyst. At 850 °C, the S/C molar feed ratio was varied. Increasing the S/C ratio enhanced catalyst durability. Figure 8a shows how running with an S/C molar feed ratio of 3 catalytic activity was largely maintained after 100 h of testing (some initial deactivation appeared to have occurred). By comparison, only 78% of catalytic activity was maintained with a lower S/C molar feed ratio of 1.5. Thus, increasing the S/C ratio improves catalyst durability. Figure 8b shows that a reduced operation temperature has a beneficial effect on catalyst life. Even after a 500 h test duration, the Rh catalyst retained its activity when operated at 750 °C.

3. Experimental Methods

3.1. Catalyst Preparation

As reported elsewhere [20], a series of catalysts were prepared by incipient wetness impregnation of MgAl₂O₄ (Puralox 30/140 from Sasol) with a solution of Rh nitrate (10 wt.% Rh in nitric acid), Ir nitrate (19.3 wt.% Ir in nitric acid), and Ni nitrate hexahydrate salt (Sigma-Aldrich, St. Louis, MO, USA). The resulting metal loadings were 5 wt.% Rh, 5 wt.% Ir, and 15 wt.% Ni. After impregnation, the catalysts were dried at 120 °C for 8 h and calcined at 500 °C for 4 h under static air.

3.2. Catalyst Characterization

Scanning transmission electron microscopy (STEM) measurements over reduced samples (850 °C, 16 h, 10% H₂/N₂) were conducted with a FEI Titan 80–300 microscope (Hillsboro, OR, USA) operated at 300 kV. The FEI Titan is equipped with a CEOS GmbH double-hexapole aberration corrector (Heidelberg, Germany) for the probe-forming lens, which allows imaging at ~0.1 nm resolution in STEM mode. The STEM images were acquired on high angle annular dark field with an inner collection angle of 52 mrad. In general, sample preparation involved mounting powder pre-reduced samples on copper grids covered with lacey carbon support films and then loading them immediately into the instrument airlock to minimize an exposure to atmospheric O₂.

Nitrogen adsorption was measured at 77 K with an automatic adsorptiometer (Micromeritics ASAP 2000, Norcross, GA, USA). The samples were pre-treated at 383 K for 12 h under vacuum.

The surface areas were determined from adsorption values for five relative pressures (P/P_0) ranging from 0.05 to 0.2 using the Brunauer–Emmett–Teller method.

Temperature programmed reduction (TPR) and H_2 chemisorption experiments were performed using an AutoChem II 2920 automated chemisorption analyzer (Micromeritics, Norcross, GA, USA). Metal reducibility was determined by TPR using changes in a thermal conductivity signal of the effluent gas. Samples (100 mg) were heated to 800 °C at 5 °C/min in a gas stream of 5% H_2 in Ar (50 sccm). Volumetric pulse H_2 adsorption measurements were carried out at 600 °C and 800 °C. First, 50 mg of the sample was reduced at 850 °C for 16 h using H_2 (10% in N_2 , 100 mL/min) and purged for 4 h in pure N_2 . After ramping to the adsorption temperature, 5% H_2 /Ar was pulsed using a 100 μ L loop with 1 min intervals between injections.

The amount of solid carbon deposited on the spent catalysts was measured by a Shimadzu Total Carbon Analyzer (TOC-5000A with a SSM-5000A Solid Sample Module, Shimadzu, Kyoto, Japan). A 1% O_2 /Ar mixture was blown through the sample starting from 40 °C until the temperature reached 900 °C. The temperature ramping rate was 10 °C/min.

3.3. Activity Measurements

Catalytic activity tests were conducted in an 8 mm inner diameter Inconel fixed-bed reactor. For each test, the catalyst (9 mg, 60–100 mesh), diluted with α - Al_2O_3 (90 mg, 60–100 mesh), was loaded between two layers of quartz wool inside the reactor. Temperature was monitored with a thermocouple placed in the middle of the catalyst bed. Before reaction, the catalyst was reduced at 850 °C for 16 h using H_2 (10% in N_2 , 100 mL/min).

Methane, ethane and natural gas simulant (94.5% methane, 4% ethane, 1% propane, 0.5% butane) gases were supplied by Matheson (Longview, WA, USA). Deionized water (18.6 m Ω) was introduced using a high-performance liquid chromatography pump (ChromTech series 1500, Bad Camberg, Germany) through $1/16$ inch stainless steel tubing into a vaporizer where the temperature was set at 250 °C. The catalysts were tested at atmospheric pressure at temperatures ranging from 550–900 °C, over a range of gas-hour-space-velocities (22,000–356,000 h $^{-1}$). Note that we commonly refer to throughput in terms of contact time (τ) which ranges from 10–170 ms. Flow rates of dry gas products in the effluent gases were monitored by a digital flow meter (DryCal) (Mesa Labs, Butler, NJ, USA). Gas products were analyzed online using a two-channel Agilent Micro GC (3000A series) (Santa Clara, CA, USA) equipped with thermal conductivity detector.

In a typical experiment, a mass of 9 mg of catalyst was loaded to the reactor, 220 sccm of gas was fed down flow to the catalytic bed (80 sccm of N_2 , 35 sccm of methane, 105.8 sccm of H_2O [0.085 mL/min]). Under those conditions, the calculated space velocity (GHSV) was 119,223 h $^{-1}$, which corresponds to a τ of 30.2 ms and an S/C molar ratio of 3.0. For ethane reforming experiments, changes in space velocities were achieved with changes in gas flow (3.5–35 sccm of ethane for the Ir catalyst case, 35–100 sccm of ethane for Rh catalyst case) while concentrations (14.8 mol% ethane) and S/C ratios were maintained constant (S/C = 2.75).

4. Conclusions

This study compares $MgAl_2O_4$ -supported Rh and Ir catalysts for the reforming reaction of methane, ethane, and natural gas simulant (a C_1 – C_4 mixture) under industrially relevant conditions. In reforming of a natural gas simulant mixture, the Ir catalyst showed a lower capacity for converting C_{2+} hydrocarbons compared to Rh in the lower 600–700 °C range of reforming temperatures. At higher temperatures (700–900 °C), there is no real distinction in the activity for the two metals. In a more detailed study of the reaction at 600 °C, the Ir-based catalyst showed a limited capacity for ethane reforming compared to methane. Additionally, the formation of ethylene as a byproduct was accompanied by a higher amount of carbon deposited on the catalyst when ethane is used as a reactant. On the contrary, the reforming rate of ethane was faster over the Rh catalyst. Less carbon was deposited and a negligible amount of ethylene was formed. A lower reaction rate of ethane over Ir is likely

related to a lower C–C scission rate. Literature reports for ethane hydrogenolysis explain how this decreased rate depends on the nature of the metal. The kinetic study found there to be a lower reaction order for ethane reforming over Ir compared to Rh and Ni (0.29, 0.79, 0.76, respectively), which is consistent with a higher coverage of the catalysts by carbon deposits. Calculated activation energies also were found to be higher for Ir compared to Rh and Ni (95, 26, 79 kJ/mol, respectively) in the lower temperature reforming range.

Adsorbed hydrogen assists hydrocarbon reactions on metal supported catalysts by hydrogenating C₁ species to form methane. In an attempt to extend the analysis that H adsorption has on Ir and Rh reforming catalysts, we performed H₂ adsorption measurements on Ir, Rh, and Ni at reforming reaction temperatures (600 °C). Results indicate that hydrogen saturates the Rh surface in a ratio 1:1 with respect to metal atoms on the surface. Coverages over Ir and Ni were found lower (0.7:1 for Ir, and 0.2:1 for Ni). A summary of main findings is presented in Table 4.

Table 4. Summary of key findings.

| Catalyst | Metal Loading (wt.%) | Metal Dispersion (%) | Metal Particle Size (nm) | H Stoichiometry H/M _{surf} (mol/mol) | n _{Ethane} | n _{water} | E _a (kJ/mol) |
|---------------------------------------|----------------------|----------------------|--------------------------|-----------------------------------------------|---------------------|--------------------|-------------------------|
| 5Rh/MgAl ₂ O ₄ | 5 | 50 | 2.0 | 1:1 | 0.79 | 0 | 26.8 |
| 5Ir/MgAl ₂ O ₄ | 5 | 100 | 1.0 | 0.7:1 | 0.29 | −0.3 | 95.7 |
| 15Ni/MgAl ₂ O ₄ | 15 | 15.4 | 6.5 | 0.2:1 | 0.76 | 0 | 79.1 |

Given the low capacity of Ir to reform ethane and higher hydrocarbons, Rh was chosen for additional catalyst durability studies. Long-term stability tests revealed the Rh catalyst to be very stable under SMR conditions, and under relatively harsh conditions (up to 900 °C and with S/C molar feed ratios up to 1.5). However, when a more complex mixture of hydrocarbons was added to the methane feed, catalyst stability was adversely affected. Here, the S/C molar feed ratio and operating temperature can be adjusted to extend catalyst life. Stable catalyst operation was observed for the Rh catalyst when using a natural gas simulant and operating under a relatively low S/C ratio of 2.0 and at 850 °C. Thus, we note that improvements in catalyst life can be achieved through both proper choice of the catalyst material and operational conditions. In addition, temperature and S/C molar feed ratio are critical processing variables to consider when optimizing catalyst performance. The results of this study conclude that a Rh-supported catalyst was developed that enables very high activities and excellent catalytic stability for both the steam reforming of methane and other higher hydrocarbons contained in natural gas, and under conditions of operation that are amendable to solar thermochemical operations.

Supplementary Materials: The following are available online at <http://www.mdpi.com/2073-4344/9/10/801/s1>, Figure S1. (A) TEM analysis of 5Ir/MgAl₂O₄ (top) and 5Rh/MgAl₂O₄ (bottom) catalysts used in this study. (B) Effect of ageing on Rh/MgAl₂O₄ catalyst. (950 °C) under H₂. Figure S2. Hydrogen uptake at 600 and 800 °C. Evolution of hydrogen uptake is calculated as H coverage (per mole of metal surface) vs H₂ pulsed. Volumetric pulse hydrogen adsorption measurements were carried out at 600 °C and 800 °C. First, 50 mg of the sample was reduced at 850 °C for 16 h using H₂ (flow 10% in N₂, 100 mL/min) and purged for 4 in pure N₂. After ramping at the adsorption temperature, 5% Hydrogen/Ar is pulsed using a 100 µL loop with 1 minute intervals between injections. Figure S3. Conversion of the individual components of a simulant natural gas mixture. Butane conversion was complete. Reaction conditions: S/C:1.5, t = 4.5 ms, 1h TOS, Simulant gas feed (94.5%_v methane, 4% ethane, 1% propane, 0.5% butane) was supplied by Matheson. Figure S4. Ethane reforming conversion vs time on stream at 600 °C. Reaction conditions: S/C = 2.75, 9 mg of catalyst. τ = 28.3 ms, 35 sccm ethane, 80 sccm N₂, 9 mg of catalyst. Table S1. Deactivation check experiments for the Ir catalyst under ethane reforming experiments shown in Figure S4. Fresh catalyst was tested for methane activity before (“initial”) and after reaction with ethane to check for deactivation (“final”). Figure S5. Ethane reforming conversion and carbon selectivity vs contact time (ms) for the reforming of ethane at 600 °C over MgAl₂O₄-supported Ir and Rh catalysts (A-top), ethylene selectivity (mol %) vs contact time (ms) (B-middle), and linear correlation for ethane conversion vs contact time. Reaction conditions: S/C = 2.75, 9 mg of catalyst. Changes in contact time were achieved by changing gas flow over the same mass of catalyst in a continuous experiment. Each point corresponds to a steady state measurement after stabilizing for 1h. Ethane over iridium catalyst was changed from 35 to 3.5 sccm. For the case of Rh, ethane

flow was varied from 35 to 100 sccm. Figure S6. Ethane reforming conversion over 5Ir/MgAl₂O₄ catalyst at 600 °C. (A) Ethane conversion vs time on stream at increase carbon/steam ratio (10 for empty symbols) at two different concentration of ethane in the gas (8 and 14 vol %). (B) Ethane conversion vs time on stream comparing Ir activity over two different supports, MgAl₂O₄ (red) and Al₂O₃ (blue). Figure S7. (A) Product selectivity for ethane steam reforming over Ir at 600 °C (8.2% conversion). (B) Ethane conversion over Rh and Ir catalysts at 600 °C (S/C = 3 mol, τ = 28 ms (Rh), τ = 167 ms (Ir)). Figure S8. Conversion vs time on stream for methane steam reforming over the Rh and Ir supported catalysts at 850 °C (S/C = 3 mol, τ = 12.4 ms; Methane feed = 22.6 vol. %). Figure S9. Methane conversion (A) and H₂/CO ratio for methane steam reforming products (B) over benchmark 5% Rh/MgAl₂O₄ catalyst. CH₄, S/C = 3, 9 mg of catalyst. 5% Rh MgAl₂O₄ catalyst reduced in-situ at 850 °C for 16 h under flowing 10% H₂ in N₂.

Author Contributions: Conceptualization, J.S.L., R.A.D. and V.L.D.; Methodology, R.A.D., V.L.D., L.K., and J.S.L.; Investigation, J.S.L., V.L.D., L.K. and C.A.D.; Data Curation and Formal Analysis, J.S.L. and R.A.D.; Writing—Original Draft Preparation, J.S.L.; Writing—Review & Editing and Supervision, R.A.D.; Project Administration and Funding Acquisition, R.A.D. and R.S.W.

Funding: This work was financially supported by the U.S. Department of Energy's (DOE) Solar Energy Technology Office (SETO) and was performed at the Pacific Northwest National Laboratory (PNNL) under Contract DE-AC05-76RL01830.

Acknowledgments: Catalyst characterization equipment use was granted by a user proposal at the William R. Wiley Environmental Molecular Sciences Laboratory, which is a national scientific user facility sponsored by the DOE Office of Biological and Environmental Research and located at PNNL. The authors would like to thank David L. King for offering a technical review and Cary A. Counts for providing technical editing support of this manuscript. The views and opinions of the authors expressed herein do not necessarily state or reflect those of the United States Government or any agency thereof. Neither the United States Government nor any agency thereof, nor any of their employees, makes any warranty, expressed or implied, or assumes any legal liability or responsibility for the accuracy, completeness, or usefulness of any information, apparatus, product, or process disclosed, or represents that its use would not infringe privately owned rights.

Conflicts of Interest: The authors declare no conflict of interest.

References

1. Nikolaidis, P.; Poullikkas, A. A comparative overview of hydrogen production processes. *Renew. Sustain. Energy Rev.* **2017**, *67*, 597–611. [CrossRef]
2. DOE. Hydrogen Production: Natural Gas Reforming, Washington, DC, USA. Available online: <https://www.energy.gov/eere/fuelcells/hydrogen-production-natural-gas-reforming> (accessed on 23 April 2019).
3. Azizi, Z.; Rezaeimanesh, M.; Tohidian, M.R. Rahimpour, Dimethyl ether: A review of technologies and production challenges. *Chem. Eng. Process. Process Intensif.* **2014**, *82*, 150–172. [CrossRef]
4. Wood, D.A.; Nwaoha, C.; Towler, B.F. Gas-to-liquids (GTL): A review of an industry offering several routes for monetizing natural gas. *J. Nat. Gas Sci. Eng.* **2012**, *9*, 196–208. [CrossRef]
5. Glasser, D.; Hildebrandt, D.; Liu, X.; Lu, X.; Masuku, C.M. Recent advances in understanding the Fischer–Tropsch synthesis (FTS) reaction. *Curr. Opin. Chem. Eng.* **2012**, *1*, 296–302. [CrossRef]
6. Pakhare, D.; Spivey, J. A review of dry (CO₂) reforming of methane over noble metal catalysts. *Chem. Soc. Rev.* **2014**, *43*, 7813–7837. [CrossRef] [PubMed]
7. Jones, G.; Jakobsen, J.; Shim, S.; Kleis, J.; Andersson, M.; Rossmeis, J.; Abildpedersen, F.; Bligaard, T.; Helveg, S.; Hinnemann, B.; et al. First principles calculations and experimental insight into methane steam reforming over transition metal catalysts. *J. Catal.* **2008**, *259*, 147–160. [CrossRef]
8. Zheng, R.; Diver, R.; Caldwell, D.; Fritz, B.; Cameron, R.; Humble, P.; TeGrotenhuis, W.; Dagle, R.; Wegeng, R. Integrated Solar Thermochemical Reaction System for Steam Methane Reforming. *Energy Procedia* **2015**, *69*, 1192–1200. [CrossRef]
9. Simakov, D.S.A.; Wright, M.M.; Ahmed, S.; Mokheimer, E.M.A.; Román-Leshkov, Y. Solar thermal catalytic reforming of natural gas: A review on chemistry, catalysis and system design. *Catal. Sci. Technol.* **2015**, *5*, 1991–2016. [CrossRef]
10. Steinfel, A. Solar thermochemical production of hydrogen—A review. *Sol. Energy* **2005**, *78*, 603–615. [CrossRef]
11. Wang, Y.; Chin, Y.H.; Rozmiarek, R.T.; Johnson, B.R.; Gao, Y.; Watson, J.; Tonkovich, A.Y.L.; Wiel, D.P.V. Highly active and stable Rh/MgOAl₂O₃ catalysts for methane steam reforming. *Catal. Today* **2004**, *98*, 575–581. [CrossRef]

12. Palo, D.R.; Stenkamp, V.S.; Dagle, R.A.; Jovanovic, G.N. Industrial Applications of Microchannel Process Technology in the United States. In *Micro Process Engineering*; Kockmann, N., Ed.; WILEY-VCH Verlag GmbH & Co. KGaA: Weinheim, Germany, 2008; pp. 387–414.
13. Kehres, J.; Andreasen, J.W.; Fløystad, J.B.; Liu, H.; Molenbroek, A.; Jakobsen, J.G.; Chorkendorff, I.; Nielsen, J.H.; Høydalsvik, K.; Breiby, D.W.; et al. Reduction of a Ni/Spinel Catalyst for Methane Reforming. *J. Phys. Chem. C* **2015**, *119*, 1424–1432. [[CrossRef](#)]
14. Salhi, N.; Boulahouache, A.; Petit, C.; Kiennemann, A.; Rabia, C. Steam reforming of methane to syngas over NiAl₂O₄ spinel catalysts. *Int. J. Hydrog. Energy* **2011**, *36*, 11433–11439. [[CrossRef](#)]
15. Boukha, Z.; Jiménez-González, C.; de Rivas, B.; González-Velasco, J.R.; Gutiérrez-Ortiz, J.I.; López-Fonseca, R. Synthesis, characterisation and performance evaluation of spinel-derived Ni/Al₂O₃ catalysts for various methane reforming reactions. *Appl. Catal. B Environ.* **2014**, *158–159*, 190–201. [[CrossRef](#)]
16. Aramouni, N.A.K.; Touma, J.G.; Tarboush, B.A.; Zeaiter, J.; Ahmad, M.N. Catalyst design for dry reforming of methane: Analysis review. *Renew. Sustain. Energy Rev.* **2018**, *82*, 2570–2585. [[CrossRef](#)]
17. Ligthart, D.A.J.M.; van Santen, R.A.; Hensen, E.J.M. Influence of particle size on the activity and stability in steam methane reforming of supported Rh nanoparticles. *J. Catal.* **2011**, *280*, 206–220. [[CrossRef](#)]
18. Duarte, R.B.; Krumeich, F.; van Bokhoven, J.A. Structure, Activity, and Stability of Atomically Dispersed Rh in Methane Steam Reforming. *ACS Catal.* **2014**, *4*, 1279–1286. [[CrossRef](#)]
19. Mei, D.; Lebarbier, V.M.; Rousseau, R.; Glezakou, V.-A.; Albrecht, K.O.; Kovarik, L.; Flake, M.; Dagle, R.A. Comparative Investigation of Benzene Steam Reforming over Spinel Supported Rh and Ir Catalysts. *ACS Catal.* **2013**, *3*, 1133–1143. [[CrossRef](#)]
20. Mei, D.; Glezakou, V.-A.; Lebarbier, V.; Kovarik, L.; Wan, H.; Albrecht, K.O.; Gerber, M.; Rousseau, R.; Dagle, R.A. Highly active and stable MgAl₂O₄-supported Rh and Ir catalysts for methane steam reforming: A combined experimental and theoretical study. *J. Catal.* **2014**, *316*, 11–23. [[CrossRef](#)]
21. Dagle, V.L.; Dagle, R.; Kovarik, L.; Genc, A.; Wang, Y.-G.; Bowden, M.; Wan, H.; Flake, M.; Glezakou, V.-A.; King, D.L.; et al. Steam reforming of hydrocarbons from biomass-derived syngas over MgAl₂O₄-supported transition metals and bimetallic IrNi catalysts. *Appl. Catal. B Environ.* **2016**, *184*, 142–152. [[CrossRef](#)]
22. Speight, J.G. *Composition and Properties, Natural Gas—A Basic Handbook*; Gulf Publishing Company: Houston, TX, USA, 2007.
23. U.S.E.I. Administration. *Ethane Production Growth Led to Record U.S. Natural Gas Plant Liquids Production in 2017, 2018*; US Energy Initiatives Corporation: Santa Clarita, CA, USA, 2018.
24. Adesina, A.A.; Trimm, D.L.; Cant, N.W. Kinetic study of iso-octane steam reforming over a nickel-based catalyst. *Chem. Eng. J.* **2004**, *99*, 131–136.
25. Sperle, T.; Chen, D.; Lødeng, R.; Holmen, A. Pre-reforming of natural gas on a Ni catalyst. *Appl. Catal. A Gen.* **2005**, *282*, 195–204. [[CrossRef](#)]
26. Takeguchi, T.; Kani, Y.; Yano, T.; Kikuchi, R.; Eguchi, K.; Tsujimoto, K.; Uchida, Y.; Ueno, A.; Omoshiki, K.; Aizawa, M. Study on steam reforming of CH₄ and C₂ hydrocarbons and carbon deposition on Ni-YSZ cermets. *J. Power Sources* **2002**, *112*, 588–595. [[CrossRef](#)]
27. Jeong, H.; Kang, M. Hydrogen production from butane steam reforming over Ni/Ag loaded MgAl₂O₄ catalyst. *Appl. Catal. B Environ.* **2010**, *95*, 446–455. [[CrossRef](#)]
28. Baek, B.; Aboiralor, A.; Wang, S.; Kharidehal, P.; Grabow, L.C.; Massa, J.D. Strategy to improve catalytic trend predictions for methane oxidation and reforming. *AIChE J.* **2017**, *63*, 66–77. [[CrossRef](#)]
29. Angeli, S.D.; Monteleone, G.; Giaconia, A.; Lemonidou, A.A. State-of-the-art catalysts for CH₄ steam reforming at low temperature. *Int. J. Hydrog. Energy* **2014**, *39*, 1979–1997. [[CrossRef](#)]
30. Halabi, M.H.; de Croon, M.H.J.M.; van der Schaaf, J.; Cobden, P.D.; Schouten, J.C. Low temperature catalytic methane steam reforming over ceria–zirconia supported rhodium. *Appl. Catal. A Gen.* **2010**, *389*, 68–79. [[CrossRef](#)]
31. Morlanés, N. Reaction mechanism of naphtha steam reforming on nickel-based catalysts, and FTIR spectroscopy with CO adsorption to elucidate real active sites. *Int. J. Hydrog. Energy* **2013**, *38*, 3588–3596. [[CrossRef](#)]
32. Wei, J. Structural requirements and reaction pathways in methane activation and chemical conversion catalyzed by rhodium. *J. Catal.* **2004**, *225*, 116–127. [[CrossRef](#)]
33. Kneale, B.; Ross, J.R.H. The steam reforming of ethane over nickel/alumina catalysts. *Faraday Discuss. Chem. Soc.* **1981**, *72*, 157–171. [[CrossRef](#)]

34. Graf, P.O.; Mojet, B.L.; van Ommen, J.G.; Lefferts, L. Comparative study of steam reforming of methane, ethane and ethylene on Pt, Rh and Pd supported on yttrium-stabilized zirconia. *Appl. Catal. A Gen.* **2007**, *332*, 310–317. [[CrossRef](#)]
35. Schädel, B.T.; Duisberg, M.; Deutschmann, O. Steam reforming of methane, ethane, propane, butane, and natural gas over a rhodium-based catalyst. *Catal. Today* **2009**, *142*, 42–51. [[CrossRef](#)]
36. Wei, J.; Iglesia, E. Mechanism and Site Requirements for Activation and Chemical Conversion of Methane on Supported Pt Clusters and Turnover Rate Comparisons among Noble Metals. *J. Phys. Chem. B* **2004**, *108*, 4094–4103. [[CrossRef](#)]
37. Mei, D.; Dagle, V.L.; Xing, R.; Albrecht, K.O.; Dagle, R.A. Steam Reforming of Ethylene Glycol over MgAl₂O₄ Supported Rh, Ni, and Co Catalysts. *ACS Catal.* **2016**, *6*, 315–325. [[CrossRef](#)]
38. Xing, R.; Dagle, V.L.; Flake, M.; Kovarik, L.; Albrecht, K.O.; Deshmane, C.; Dagle, R.A. Steam reforming of fast pyrolysis-derived aqueous phase oxygenates over Co, Ni, and Rh metals supported on MgAl₂O₄. *Catal. Today* **2016**, *269*, 166–174. [[CrossRef](#)]
39. Huang, C.; Ma, Z.; Miao, C.; Yue, Y.; Hua, W.; Gao, Z. Catalytic decomposition of N₂O over Rh/Zn–Al₂O₃ catalysts. *RSC Adv.* **2017**, *7*, 4243–4252. [[CrossRef](#)]
40. Mizuno, T.; Matsumura, Y.; Nakajima, T.; Mishima, S. Effect of support on catalytic properties of Rh catalysts for steam reforming of 2-propanol. *Int. J. Hydrog. Energy* **2003**, *28*, 1393–1399. [[CrossRef](#)]
41. Flaherty, D.W.; Hibbitts, D.D.; Gürbüz, E.I.; Iglesia, E. Theoretical and kinetic assessment of the mechanism of ethane hydrogenolysis on metal surfaces saturated with chemisorbed hydrogen. *J. Catal.* **2014**, *311*, 350–356. [[CrossRef](#)]
42. Hernández-Cristóbal, O.; Díaz, G.; Gómez-Cortés, A. Effect of the Reduction Temperature on the Activity and Selectivity of Titania-Supported Iridium Nanoparticles for Methylcyclopentane Reaction. *Ind. Eng. Chem. Res.* **2014**, *53*, 10097–10104. [[CrossRef](#)]
43. Kip, B.J.; van Grondelle, J.; Martens, J.H.A.; Prins, R. Preparation and characterization of very highly dispersed iridium on Al₂O₃ and SiO₂. *Appl. Catal.* **1986**, *26*, 353–373. [[CrossRef](#)]
44. Nuernberg, G.D.B.; Fajardo, H.V.; Foletto, E.L.; Hickel-Probst, S.M.; Carreño, N.L.V.; Probst, L.F.D.; Barrault, J. Methane conversion to hydrogen and nanotubes on Pt/Ni catalysts supported over spinel MgAl₂O₄. *Catal. Today* **2011**, *176*, 465–469. [[CrossRef](#)]
45. Horváth, A.; Guzzi, L.; Kocsonya, A.; Sáfrán, G.; la Parola, V.; Liotta, L.F.; Pantaleo, G.; Venezia, A.M. Sol-derived AuNi/MgAl₂O₄ catalysts: Formation, structure and activity in dry reforming of methane. *Appl. Catal. A Gen.* **2013**, *468*, 250–259. [[CrossRef](#)]
46. Gillan, C.; Fowles, M.; French, S.; Jackson, S.D. Ethane Steam Reforming over a Platinum/Alumina Catalyst: Effect of Sulfur Poisoning. *Ind. Eng. Chem. Res.* **2013**, *52*, 13350–13356. [[CrossRef](#)]
47. Latimer, A.A.; Kulkarni, A.R.; Aljama, H.; Montoya, J.H.; Yoo, J.S.; Tsai, C.; Abild-Pedersen, F.; Studt, F.; Nørskov, J.K. Understanding trends in C–H bond activation in heterogeneous catalysis. *Nat. Mater.* **2016**, *16*, 225. [[CrossRef](#)] [[PubMed](#)]
48. Blanksby, S.J.; Ellison, G.B. Bond Dissociation Energies of Organic Molecules. *Acc. Chem. Res.* **2003**, *36*, 255–263. [[CrossRef](#)]
49. Burch, R.; Loader, P.K.; Urbano, F.J. Some aspects of hydrocarbon activation on platinum group metal combustion catalysts. *Catal. Today* **1996**, *27*, 243–248. [[CrossRef](#)]
50. Sinfelt, J.H.; Yates, D.J.C. Catalytic hydrogenolysis of ethane over the noble metals of Group VIII. *J. Catal.* **1967**, *8*, 82–90. [[CrossRef](#)]
51. Bond, G.C. Kinetics of alkane reactions on metal catalysts: Activation energies and the compensation effect. *Catal. Today* **1999**, *49*, 41–48. [[CrossRef](#)]
52. Kuz'min, I.V.; Zeigarnik, A.V. Microkinetic Modeling of Ethane Hydrogenolysis on Metals. *Kinet. Catal.* **2004**, *45*, 561–569. [[CrossRef](#)]
53. Vincent, R.S.; Lindstedt, R.P.; Malik, N.A.; Reid, I.A.B.; Messenger, B.E. The chemistry of ethane dehydrogenation over a supported platinum catalyst. *J. Catal.* **2008**, *260*, 37–64. [[CrossRef](#)]
54. Goddard, S.A.; Amiridis, M.D.; Rekoske, J.E.; Cardona-Martinez, N.; Dumesic, J.A. Kinetic simulation of heterogeneous catalytic processes: Ethane hydrogenolysis over supported group VIII metals. *J. Catal.* **1989**, *117*, 155–169. [[CrossRef](#)]
55. Mark, M.F.; Maier, W.F. CO₂-Reforming of Methane on Supported Rh and Ir Catalysts. *J. Catal.* **1996**, *164*, 122–130. [[CrossRef](#)]

56. Sinfelt, J.H. Kinetics of ethane hydrogenolysis. *J. Catal.* **1972**, *27*, 468–471. [[CrossRef](#)]
57. Sinfelt, J.H. Specificity in Catalytic Hydrogenolysis by Metals. In *Advances in Catalysis*; Eley, D.D., Pines, H., Weisz, P.B., Eds.; Academic Press: Cambridge, MA, USA, 1973; pp. 91–119.
58. Guzzi, L.; Gudkov, B.S.; Tétényi, P. The mechanism of catalytic hydrogenolysis of ethane over nickel. *J. Catal.* **1972**, *24*, 187–196. [[CrossRef](#)]
59. Kahle, L.C.S.; Roussi re, T.; Maier, L.; Delgado, K.H.; Wasserschaff, G.; Schunk, S.A.; Deutschmann, O. Methane Dry Reforming at High Temperature and Elevated Pressure: Impact of Gas-Phase Reactions. *Ind. Eng. Chem. Res.* **2013**, *52*, 11920–11930. [[CrossRef](#)]



  2019 by the authors. Licensee MDPI, Basel, Switzerland. This article is an open access article distributed under the terms and conditions of the Creative Commons Attribution (CC BY) license (<http://creativecommons.org/licenses/by/4.0/>).